

## 6B.6 LINKING OBSERVATIONS OF ZDR AND VERTICAL VELOCITY IN THE -15°C REGION DURING STRATIFORM PRECIPITATION

Jonathan M. Vogel\*, Frédéric Fabry, and Isztar Zawadzki

Department of Atmospheric and Oceanic Sciences, McGill University, Montreal, QC, Canada

### 1 INTRODUCTION AND BACKGROUND

Polarimetric radars have been widely used for identifying different hydrometeor types (e.g. rain, snow, graupel) as well as differentiating between different growth and transformation mechanisms (e.g. deposition, aggregation, riming, melting) (e.g. Kennedy and Rutledge, 2011; Andrić et al., 2013; Bechini et al., 2013; Schneebeli et al., 2013; Schrom et al., 2015; Vogel and Fabry, 2017). Identifying these regions and understanding where they occur within clouds can be useful for understanding the growth of the cloud, distribution and structure within the cloud, the formation and growth of different hydrometeors, and production of precipitation. Together, these can be also be used for improving microphysical constraints within numerical weather prediction models.

Since stratiform precipitation is generally more spatially homogenous and widespread than convective precipitation, it provides more ideal circumstances for observing these different microphysical processes. Surcel and Zawadzki (2010) initially observed the frequent occurrence of a localized velocity minima near the -15° region after compiling over 300 hours of vertically pointing radar data of stratiform weather events. Zawadzki (2013), later suggested this signature was due to an updraft associated with the level of nondivergence. Other studies have frequently observed the occurrence of an enhanced  $Z_{DR}$  signature near the -15°C isotherm attributing it to dendritic growth (e.g. Kennedy and Rutledge, 2011; Andrić et al., 2013; Bechini et al., 2013; Schneebeli et al., 2013; Schrom et al., 2015). Schrom et al. (2015) suggested the the signatures in this region could be due to the differential growth rates of two modes of crystals. Schrom and Kumjian (2016), added further support to the theory suggesting that, at temperatures colder than -15°C,

isometric crystals dominated the signatures; then, in the -15°C region, smaller crystals grow dendritically and grow faster eventually dominating the signatures of  $Z_{DR}$  and  $V_D$ .

In this study, we attempt to add insight to the theories of updrafts, crystal habits, and growth regimes in the -15°C region by combining divergence observations and velocity-azimuth display (VAD) calculations from a scanning S-band radar, vertically pointing Doppler velocity  $V_D$  and reflectivity  $Z_X$ , scanning polarimetric reflectivity  $Z_H$  and differential reflectivity  $Z_{DR}$ , and aircraft particle imagers from the GCPEX campaign.

### 2 DATA AND METHODOLOGY

#### 2.1 Radar Data Collection

Radars used in this study include the McGill S-band scanning dual-polarization radar located at the J.S. Marshall Radar Observatory in Ste-Anne de Bellevue, Quebec and the vertically pointing X-band Doppler radar (VertiX) located at the McGill Campus in downtown Montreal, Quebec. The McGill S-band radar is a 10.4 cm dual-polarization radar with a beam width of 0.83°. It completes a full PPI of 23 elevations from 0.5 to 31.2° every 5 minutes. VertiX is a vertically pointing 3.2 cm X-band Doppler radar that completes one vertical profile every 1.5 seconds. Doppler velocity spectra are also available from VertiX over a 2 minute interval. It is located at 30 km in range along the 72° azimuth of the S-band radar.

For the Montreal region, velocity and  $Z_{DR}$  signatures in the -15°C region appear to be long lived often lasting an hour or longer. Since polarimetric observations as well as VertiX measurements are prone to variability from both dynamical and microphysical processes on temporal and spatial scales on the order of 1-15 minutes or kilometers, VertiX and S-band data are averaged over periods of one hour. For this study, 45 one hour periods are used from 2012 and 2013. Additionally, to reduce vari-

\*Corresponding author address: Jonathan M. Vogel, Atmospheric and Oceanic Sciences, Burnside Hall 805 Sherbrooke Street West, Montreal, QC, Canada, H3A 0B9, e-mail: jonathan.vogel@mail.mcgill.ca

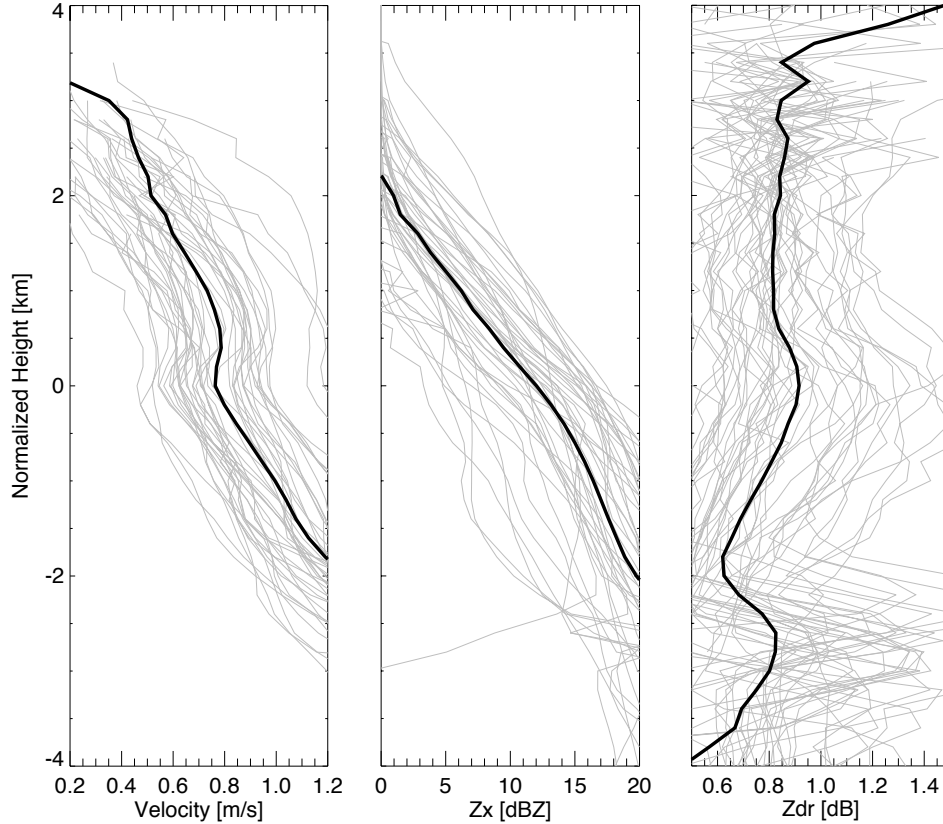


Figure 1: Vertical profiles of  $V_D$ ,  $Z_X$ , and  $Z_{DR}$  for each of the 45 cases in grey and the mean for each in black. The profiles are normalized so that the minimum in the velocity reduction is centered at 0 km.

ability and increase the vertical coverage, the polarimetric data is averaged over a region  $10^\circ$  in azimuth by 10 km in range. This region is located within 5 km of VertiX where ground clutter contamination is at a minimum; however, for data quality, any pixels with a  $Z < 0$  dBZ,  $\rho_{HV} < 0.90$ , or a target ID of "ground echo" or "biological" are removed.

## 2.2 Velocity-Azimuth Display

While many studies generally assume the vertical air motion in stratiform precipitation is small compared to the fall speeds of hydrometeors, vertical motion is required for moisture transport as well as to achieve supersaturation. Additionally, a localized updraft or an abrupt change in updraft could lead to the perviously documented observations of a sudden decrease in Doppler velocity and, therefore, hydrometeor fall speed. Due to the lack of a wind profiler and distrust in localized vertical velocities from the RAP model, another method is required to ascertain the vertical motion.

If the azimuthal coverage of Doppler velocity from

a scanning radar is sufficient at a given radius, the profile of horizontal divergence (and, therefore, vertical velocity) can be calculated. By assuming the atmosphere is in hydrostatic balance and only vertically compressible, taking the vertical derivative of the vertical wind in pressure coordinates is equal to the horizontal divergence on a constant pressure surface (O'Brien, 1970):

$$\frac{\partial \omega}{\partial p} = - \left( \frac{\partial u}{\partial x} + \frac{\partial v}{\partial y} \right)_p. \quad (1)$$

At a given radius  $r$ , the radar observed radial Doppler velocity  $V_r$  measures the air motion  $(u, v, w)$  and hydrometeor fall speed  $V_f$ :

$$V_r(r, \theta) = [u \sin(\theta) + v \cos(\theta)] \cos(\beta) + [w + V_f] \sin(\beta) \quad (2)$$

where  $\theta$  is the azimuthal angle and  $\beta$  is the elevation angle.

Because radial velocity is periodic, a least-square Fourier expansion can be used to represent the

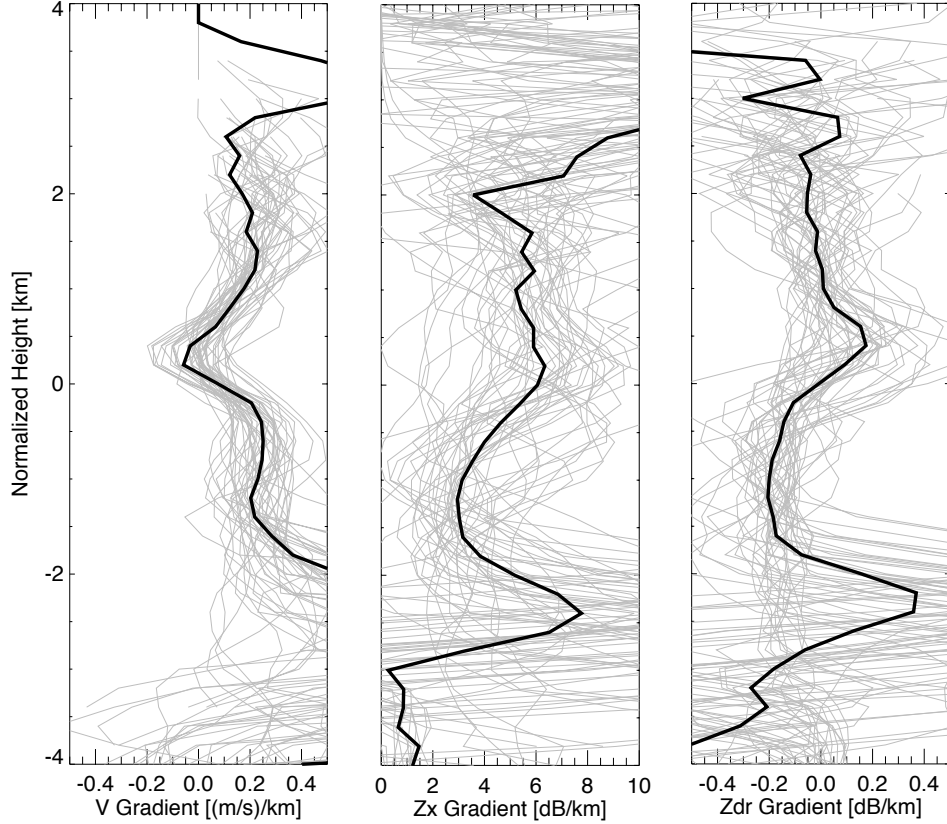


Figure 2: Vertical profiles of the gradients of  $V_D$ ,  $Z_X$ , and  $Z_{DR}$  for each of the 45 cases in grey and the mean for each in black. The profiles are normalized so that the minimum in the velocity reduction is centered at 0 km..

VAD:

$$V_r(r, \theta) - V_f \sin(\beta) = A_0 + A_1 \sin(\theta) + B_1 \cos(\theta) + A_2 \sin(2\theta) + B_2 \cos(2\theta). \quad (3)$$

The radial doppler velocity from (2) can be rewritten with the horizontal wind and its derivatives:

$$V_r(r, \theta) - V_f \sin(\beta) = \{r/2(u_x + v_y) + [u_0 \cos(\beta)] \sin(\theta) + [v_0 \cos(\beta)] \cos(\theta) + r/2(u_y - v_x) \sin(2\theta) + r/2(v_y - u_x) \cos(2\theta)\} \cos(\beta) + w \sin(\beta) \quad (4)$$

where  $u_x, v_x, u_y,$  and  $v_y$  are the partial derivatives of the horizontal wind. By comparing (3) and (4), the horizontal divergence  $\delta$  can be found using the

$A_0$  term from the Fourier expansion (Browning and Wexler, 1968):

$$\delta = (u_x + v_y) = \frac{2A_0}{r \cos(\beta)} \quad (5)$$

From (5), the divergence is sensitive to the radial distance from the radar while the vertical coverage is limited by the spacing of the elevation angles. The vertical velocity profile can be determined by assuming boundary conditions of  $\omega = 0$  at the surface and echo top as well as combining (1) and (5). VAD profiles were calculated from radii between 30 and 40 km in range which eliminate most of the ground clutter contamination, include ranges near the VertiX location, and ensure adequate vertical coverage. Additionally, sensitivity tests have shown minimal error to divergence estimates when azimuthal coverage exceeds 90%.

### 2.3 GCPEX Data

The Global Precipitation Measurement (GPM) Cold-season Precipitation Experiment (GCPEX)

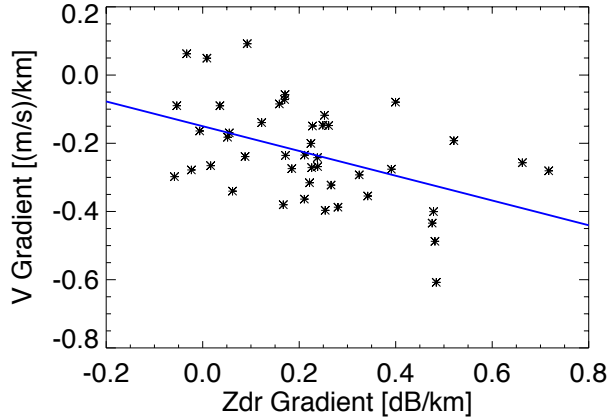


Figure 3: The normalized greatest  $Z_{DR}$  gradient and its corresponding normalized velocity gradient for each of the 45 cases

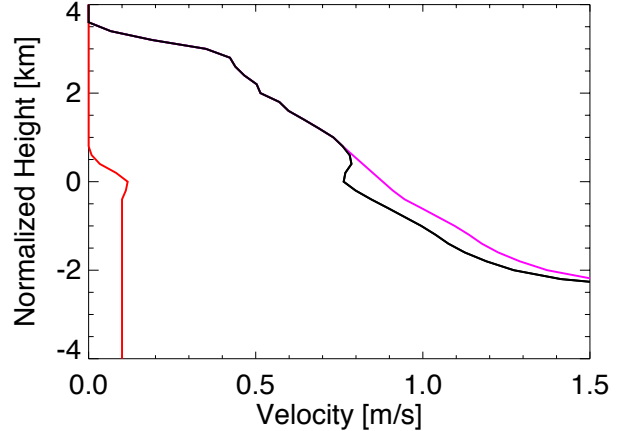


Figure 4: 45 case mean VertiX observed  $V_D$  in black, velocity profile with no reduction in magenta, and the resulting updraft required in red.

field campaign took place from January 17 to February 29, 2012 near Ontario, Canada. Among the several instruments that were involved in the mission, data was used from the University of North Dakota Cessna Citation aircraft, the University of McGill VertiX radar, and the Environment Canada King City dual-polarization C-band radar. The vertically pointing VertiX Doppler velocity data was used to find periods of local velocity minima. The Citation aircraft provided in situ measurements of temperature, moisture, saturation, number concentration, and particle imagers during vertical spirals. The King City radar provided dual-polarimetric volume scans every 10 minutes. When the Citation conducted an observation spiral within the 10 km of the VertiX, the data were combined with the nearest pixel of C-band data to determine what crystal habit or collection of crystals contributed to the signatures observed both on VertiX and on dual-polarization.

### 3 OBSERVATIONS

#### 3.1 Average Profiles from the Montreal Region

Data was collected from 45 one hour periods from the McGill VertiX and scanning S-band radars. To focus on the velocity reduction signature, all cases have been normalized in height so that the velocity minima occurs at 0 km (Figure 1). The velocity reduction occurs over a depth of about 1 km and is quite consistent from case-to-case. The peak  $Z_{DR}$  maxima occurs at the same height as the velocity minima; however, it occurs over a broader region.  $Z_{DR}$  shows more variability from case-to-case with some having an abrupt peak while others show a gradual transition from increasing to decreasing.

Figure 2 shows that the gradients, relative to towards the surface, for both velocity and  $Z_{DR}$  occur almost simultaneously, while the gradient of  $Z$  begins shortly after. The relationship between the normalized greatest  $Z_{DR}$  gradient and its corresponding normalized velocity gradient is shown in Figure 3. These values are taken from the 0-1 km normalized heights. It depicts a clear trend of increasing  $Z_{DR}$  growth corresponding with a greater velocity reduction. To obtain the normalized velocity and  $Z_{DR}$  gradients, the normalization factor is calculated from the mean of velocity and  $Z_{DR}$  gradients in the 1-2 km normalized height region. This normalization factor is then subtracted from the entire profile. This is necessary to remove any background growth rates in both velocity and  $Z_{DR}$  and observe the absolute change immediately above the 0 km normalized height.

#### 3.2 GCPEX Cases

Combining the vertically pointing VertiX data for velocity and  $Z$ , the King City C-band radar for  $Z_{DR}$ , and in situ particle imager observations from the Citation aircraft, a three (CHECK THIS) cases could be compiled of observations during a spiral by the Citation. One example is presented here for brevity, which represents the typical observations from all the cases (Figure 7). At temperatures cooler than  $-15^\circ\text{C}$ , generally around  $-20^\circ\text{C}$ , VertiX shows  $Z$  less than 10 dBZ and  $V_D$  up to  $1.0 \text{ m s}^{-1}$ .  $Z_{DR}$  values from the C-band radar are generally around 0.50 dB. The particle imager shows a collection of bullets, needles, and rosettes; generally, smaller crystals with larger area ratio values and lower drag.

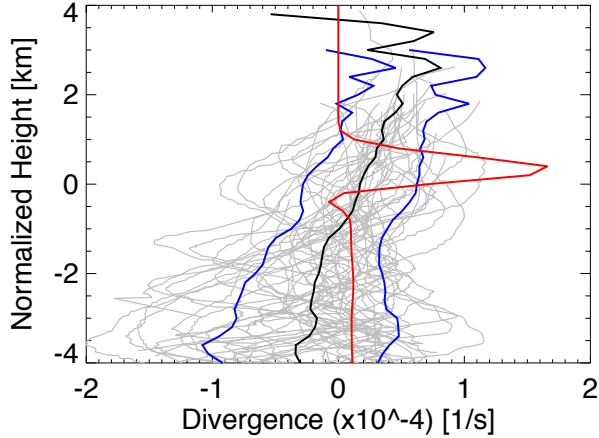


Figure 5: 45 case mean divergence (in black) calculated from VAD observations  $\pm 1$  standard deviation (in blue). Grey lines show the divergence profiles for each of the 45 cases. The red line is the expected divergence signature for updraft (red line) shown in Figure 4.

Area ratio is defined as the area an ice crystal takes up over a circumscribed disk, so a value of 1 means the crystal fills the whole disk while a value closer to 0 generally means a more porous crystal. At lower altitudes, the temperature is closer to  $-15^{\circ}\text{C}$  and vertiX shows an increase in  $Z$  to about 10 dBZ and a decrease in  $V_D$  to about  $0.8 \text{ m s}^{-1}$  coinciding with an increase in  $Z_{DR}$  to about 0.75 to 0.8 dB. At this time, the Citation particle imager observes larger and more complex crystals: crystals with dendritic-like appendages, capped columns, and some dendrites, all of which have lower area ratio values and more drag than what was observed above. Then, as temperatures rise about  $-15^{\circ}\text{C}$ ,  $Z$  increases above 10 dBZ and  $V_D$  increases back to  $1.0 \text{ m s}^{-1}$  coinciding with  $Z_{DR}$  decreasing below 0.75 dB. The Citation particle image shows the presence of even larger crystals with varying complexity with a majority being aggregates of what was observed above with area ratios also higher than what was observed around  $-15^{\circ}\text{C}$ .

## 4 DISCUSSION

### 4.1 Localized Updraft

Zawadzki (2013), suggested that the sudden slowdown in velocity observed by all crystals in the velocity spectra requires a localized updraft to be present. For the 45 one hour periods collected, the mean vertical velocity profile was determined by normalizing the height for each case to the height of the velocity minima (black line, Figure 4). As-

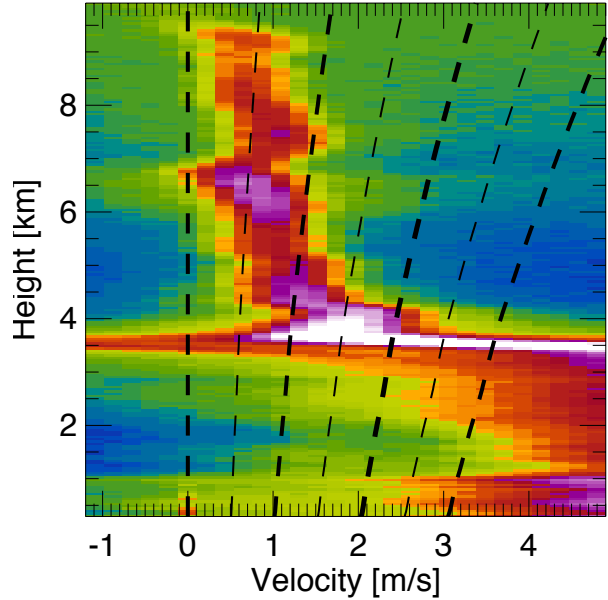


Figure 6: Example velocity spectra taken from a 2 minute sample during one of the 45 cases. The abrupt velocity slow down is apparent around 7 km which is also  $-15^{\circ}\text{C}$  for this case.

suming an updraft is the cause of this velocity reduction, the resulting updraft is shown in red on Figure 4. By continuity, for an updraft, or change in updraft speed, to be present of this magnitude a corresponding convergence/divergence signature should be discernible from VAD observations. By (1), the expected divergence profile can be calculated (red line, Figure 5).

Figure 5 shows that the expected divergence signature (in red) occurs over a vertical depth of about 1 km. In Montreal, the velocity reduction often occurs near a height of 5 km. Near this altitude, a VAD profile at a single radius could miss such a narrow signature due to the lack of vertical coverage at higher elevations. However, by combining VAD profiles at several successive ranges the lack of vertical coverage is mitigated. Figure 5 shows that on average the divergence profile (in black) indicates a broad updraft spanning several kilometers. While a few cases could have a localized updraft that results in uniform slowing of falling crystals, on average it is unlikely to be the source of this common velocity reduction signature. However, the VAD profiles do show the presence, on average, of a broad updraft which provides the necessary ingredients for enhanced depositional growth in this region.

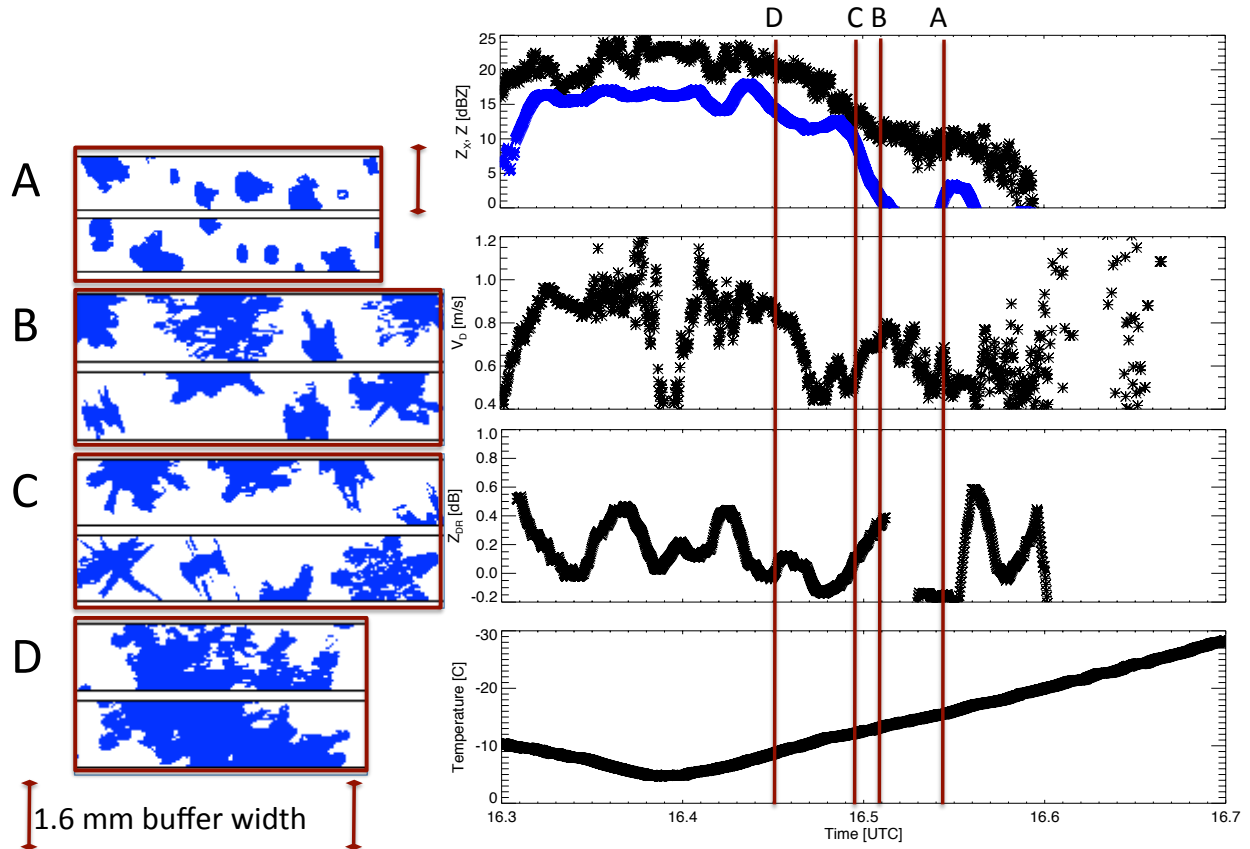


Figure 7: GCPEX data during an aircraft spiral from 16z on February 18, 2012. On the right, from top to bottom, is  $Z$  (VertiX in black, King City C-band in blue), VertiX  $V_D$ , King City  $Z_{DR}$ , and temperature observations from the Citation aircraft ambient temperature probe. A, B, C, and D on the left correspond to Citation 2D-C particle images with a 1.6 mm buffer width during the corresponding times shown on the right.

## 4.2 Two Crystal Habits

Schrom et al. (2015) and Schrom and Kumjian (2016), observed positive gradients in  $Z$  and  $Z_{DR}$  and a negative gradient in  $V$ , all relative to decreasing height, and attributed them to differential growth between two crystal habits. Aloft, faster falling more isometric crystals dominate the reflectivity weighted products. As they enter the  $-15^\circ\text{C}$  region, the smaller crystals grow faster than the larger preexisting ones. Based on the Bailey and Hallett (2009) habit diagram, they will grow dendritically which will fall slower and contribute to a positive  $Z_{DR}$  signature. As they grow large enough they will dominate the reflectivity weighted products producing the observed signatures.

Figure 6 shows a typical velocity spectra observed by VertiX during the 45 on hour periods. The lack of a bimodal spectra within the  $-15^\circ\text{C}$  region where the velocity slows suggests the lack of two different habits of crystals or the preexisting crys-

tals are now falling at the same velocity as any new crystals that are produced. While it is possible for an occasional bimodal spectra to be observed within the  $-15^\circ\text{C}$  region, the lack of it regularly occurring while other signatures of present suggests it is unlike to be the common source of the signature.

## 4.3 Microphysical Growth

From the 45 one hour cases, Figures 1, 2, and 3 show support of a relationship between velocity decreasing while  $Z$  and  $Z_{DR}$  are increasing. Citation aircraft particle images from the GCPEX campaign show a distinct change in crystal type when moving from temperatures colder than  $-15^\circ\text{C}$ , to the  $-15^\circ\text{C}$  region, to temperatures warmer than  $-15^\circ\text{C}$  coinciding with these radar observations. It has been previously theorized that  $Z_{DR}$  signatures in the  $-15^\circ\text{C}$  region are likely caused by dendrites based on the Bailey and Hallett (2009) habit diagram. Observations from the Citation aircraft support this theory

as dendritic-like growth was observed in this region (Figure 7).

Dendritic growth can be supported by all previously discussed observations. VAD observations show a broad updraft that, while is too broad to suddenly slow all crystals at this altitude, would provide the necessary moisture to reach supersaturation with respect to ice. Crystals that grow dendritically would have higher drag than those seen above which would, at least initially, lead to a reduction in velocity. Dendrites and dendritic growth would increase  $Z$  while also leading to higher  $Z_{DR}$  values than that of the ice crystals observed above. Once the ice crystals grow large enough or begin to aggregate the velocity will once again continue to increase. Once aggregation dominates the growth,  $Z_{DR}$  values will also begin to decrease. These transitions between different ice crystal growth habits were observed during vertical spirals by the Citation aircraft during the GCPEX campaign.

## 5 SUMMARY AND CONCLUSIONS

By combining observations from a vertically pointing Doppler X-band radar, scanning polarimetric S-band radar, scanning polarimetric C-band radar, and in situ data from a particle imager on a Citation aircraft new evidence has been provided to several theories to what is occurring in the  $-15^{\circ}\text{C}$  region in stratiform precipitation. Divergence and vertical velocity calculated from velocity-azimuth display data from the S-band radar show the presence of an updraft that provides moisture for depositional growth. The observed updraft and divergence signatures are much broader than expected for a localized updraft to be uniformly slowing all falling ice crystals. The lack of a regular appearance of bimodal spectra in the  $-15^{\circ}\text{C}$  region suggests that two habits of crystals growing at different rates leading to different habits dominating the reflectivity weighted products is unlikely to produce the observed  $V_D$  and  $Z_{DR}$  observations. Finally, velocity reduction coincident with  $Z$  and  $Z_{DR}$  suggest enhanced microphysical growth is producing these signatures. In situ particle images above, in, and below this region shows evidence distinct changes in dominant crystal growth habits further supporting the microphysical growth theory.

## ACKNOWLEDGEMENTS

This project was undertaken with the financial support of the Government of Canada provided

through the Department of Environment and Climate Change and the Natural Sciences and Engineering Research Council of Canada. We would like to thank Alamelu Kilambi for help accessing the McGill radar data and Bernat Puigdomènech Tre-serras for use of the Profilers application for VertiX and S-band data.

## REFERENCES

- Andrić, J., M. R. Kumjian, D. S. Zrnić, J. M. Straka, and V. M. Melnikov, 2013: Polarimetric signatures above the melting layer in winter storms: An observational and modeling study. *J. Appl. Meteor. Climatol.*, **52**, 682–700, doi:10.1175/JAMC-D-12-028.1.
- Bailey, M. P., and J. Hallett, 2009: A comprehensive habit diagram for atmospheric ice crystals: Confirmation from the laboratory, AIRS II, and other field studies. *J. Atmos. Sci.*, **66**, 2888–2899, doi:10.1175/2009JAS2883.1.
- Bechini, R., L. Baldini, and V. Chandrasekar, 2013: Polarimetric radar observations in the ice region of precipitating clouds at C-band and X-band radar frequencies. *J. Appl. Meteor. Climatol.*, **52**, 1147–1169, doi:10.1175/JAMC-D-12-055.1.
- Browning, K. A., and R. Wexler, 1968: The determination of kinematic properties of a wind field using doppler radar. *Journal of Applied Meteorology*, **7** (1), 105–113, doi:10.1175/1520-0450(1968)007<0105:TDOKPO>2.0.CO;2, URL [https://doi.org/10.1175/1520-0450\(1968\)007<0105:TDOKPO>2.0.CO;2](https://doi.org/10.1175/1520-0450(1968)007<0105:TDOKPO>2.0.CO;2), [https://doi.org/10.1175/1520-0450\(1968\)007<0105:TDOKPO>2.0.CO;2](https://doi.org/10.1175/1520-0450(1968)007<0105:TDOKPO>2.0.CO;2).
- Kennedy, P. C., and S. A. Rutledge, 2011: S-band dual-polarization radar observations of winter storms. *J. Appl. Meteor. Climatol.*, **50**, 844–858, doi:10.1175/2010JAMC2558.1.
- O'Brien, J. J., 1970: Alternative solutions to the classical vertical velocity problem. *Journal of Applied Meteorology*, **9** (2), 197–203, doi:10.1175/1520-0450(1970)009<0197:ASTTCV>2.0.CO;2, URL [https://doi.org/10.1175/1520-0450\(1970\)009<0197:ASTTCV>2.0.CO;2](https://doi.org/10.1175/1520-0450(1970)009<0197:ASTTCV>2.0.CO;2), [https://doi.org/10.1175/1520-0450\(1970\)009<0197:ASTTCV>2.0.CO;2](https://doi.org/10.1175/1520-0450(1970)009<0197:ASTTCV>2.0.CO;2).
- Schneebeli, M., N. Dawes, M. Lehning, and A. Berne, 2013: High-resolution vertical profiles of X-band polarimetric radar observables during

- snowfall in the Swiss Alps. *J. Appl. Meteor. Climatol.*, **52**, 378–394, doi:10.1175/JAMC-D-12-015.1.
- Schrom, R. S., and M. R. Kumjian, 2016: Connecting microphysical processes in colorado winter storms with vertical profiles of radar observations. *Journal of Applied Meteorology and Climatology*, **55** (8), 1771–1787, doi:10.1175/JAMC-D-15-0338.1, URL <https://doi.org/10.1175/JAMC-D-15-0338.1>, <https://doi.org/10.1175/JAMC-D-15-0338.1>.
- Schrom, R. S., M. R. Kumjian, and Y. Lu, 2015: Polarimetric radar signatures of dendritic growth zones within colorado winter storms. *J. Appl. Meteor. Climatol.*, **54** (12), 2365–2388, doi:10.1175/JAMC-D-15-0004.1.
- Surcel, M., and I. Zawadzki, 2010: Exploring snow microphysics with vertex. *Proc. Sixth European Conf. on Radar Meteorology*, Sibiu, Romania, P18.13.
- Vogel, J. M., and F. Fabry, 2017: Contrasting polarimetric observations of stratiform riming and non-riming events. *J. Appl. Meteor. Climatol.*, **Under Review**.
- Zawadzki, I., 2013: Observations of snow growth by a vertically pointing radar. *36th Conference on Radar Meteorology*, Breckenridge, CO, USA, 11A.6 [Available online at <https://ams.confex.com/ams/36Radar/webprogram/Paper229071.html>].